Applied Nanoscience
https://doi.org/10.1007/s13204-019-01118-x

ORIGINAL ARTICLE

Highly tuned cobalt-doped MnO_2 nanozyme as remarkably efficient uricase mimic

Mira V. Parmekar[1] · **A. V. Salker**[1]

Received: 7 June 2019 / Accepted: 22 July 2019

Abstract

Gouty arthritis is a commonly occurring metabolic disorder in adult humans. It is caused by accumulation of uric acid (UA) in the joints owing to lack of any enzyme like uricase, which can metabolise excess UA in the human body. In this work, we propose a solution for the same. After testing the oxidase-like activity of Co-doped MnO_2 using 3,3′,5,5′-tetramethylbenzidine (TMB), as less as 50 µg mL^{-1} of this catalyst was found to readily oxidise and completely degrade a 50 µM uric acid solution at 37 °C within 4 h (pH 7.4). The rate of the reaction found to be 1.208×10^{-4} s^{-1} at this temperature. The result clearly indicates better activity of these nanoparticles over bacterial uricase enzyme as the activation energy of the reaction decreased from the reported value of 53 to 43 kJ mol^{-1} in this work. This is by far the lowest reported E_{act} by any enzyme mimic for uricase. Composed of two bio-relevant metals namely Mn and Co, the nanozyme is economical as well as safe to use for treatment of gout. The nanozyme could be successfully recycled four times with no loss in the oxidase-like activity and proved to be quite stable in the employed conditions as the metal content and morphology were retained even after reuse. Generation of in situ singlet oxygen/superperoxide radical-type species was another striking feature of the employed nanozyme. LC–MS data of the degraded products further gave insights on the pathway followed for degradation over the nanozyme. Overall, a bio-relevant as well as cost effective alternate for the treatment of gout envisaged in the current study.

Keywords Nanozyme · Oxidase · Uric acid · Uricase · Nano-catalysis · Manganese dioxide · Singlet oxygen

Introduction

Uric acid (UA) is the most abundant antioxidant in human plasma and accounts for scavenging up to 60% of serum free-radicals which include peroxy and hydroxyl radicals, NO, NO_2 and CO_3^{2-} ions (Gersch et al. 2008). For this reason, it was previously hypothesised that these antioxidant properties of UA might be protective against oxidative stress; oxidative injury of cardiac/vascular/neural cells, ageing, etc., but the recent findings have shown conflicting observations. Hyperuricaemia—a condition of high serum uric acid, is suggested to be a risk factor for cardiovascular diseases and is frequently associated with malignancies, polycythaemia vera, haemolytic anaemia, etc, (Lippi et al. 2008). In addition, it is proposed to be a mediator for inflammatory response to injured and dying tissues (Shi et al. 2003). Chronic hyperuricemia is also associated with endothelial dysfunction and reduction in NO, which is established as one of the most important cardiovascular, nervous and immune system regulatory molecule (Gersch et al. 2008). In many cases, accumulation of UA in the joints is observed especially in toes, knees, ankles, etc., leading to a painful condition termed gout or gouty arthritis. If untreated, deposition of these monosodium urate crystals in and subcutaneous tissue of gouty joint leads to formation of hard lumps called tophi (Perez-ruiz et al. 2002). This may perforate the overlying skin, producing draining sinuses, which often become infected. High levels of UA may also cause calcium oxalate stones or kidney stones due to UA-induced crystallisation of calcium salts (Abate et al. 2004). In nature, the enzyme uricase is responsible for oxidation of uric acid

Electronic supplementary material The online version of this article (https://doi.org/10.1007/s13204-019-01118-x) contains supplementary material, which is available to authorized users.

✉ Mira V. Parmekar
mira.parmekar@gmail.com

✉ A. V. Salker
sal_arun@rediffmail.com

[1] Department of Chemistry, Goa University, Taleigao, Goa, India 403206

Published online: 02 August 2019

to allantoin which is a water-soluble unlike UA (Usuda et al. 1994). A recent discovery though has suggested existence of a series of enzymes closely working to bring about the conversion (Ramazzina et al. 2006). As nature would favour it, this enzyme is absent in humans. Therefore, the sole way to remove excess uric acid from the body is excretion.

Enzymes make highly efficient catalyst owing to its substrate selectivity and specificity. For the same reason, they are majorly used in plausible commercial applications such as sewage treatment, textile finishing, food and beverage production and even energy conservation (Wei and Wang 2008; Zhou et al. 2013). On the contrary, however, their extreme sensitivity towards external environmental conditions of pH, temperature and lack of means of mass production limits their use.

Nanomaterials, especially functional ones have received considerable attention in recent years (Polshettiwar and Varma 2010; Wei and Wang 2013). Si for example is in high demand in the electronic industry. Apart from amorphous and crystalline forms of Si, nanostructured Si which is a transformation between both the states, have influential mechanical, optical, electrical, and electrochemical properties which improves the performance of related devices (Zhang et al. 2017; Wang et al. 2018). Thus, studies related to their machining and manufacture by grinding, chemical mechanical polishing and electrochemical polishing are in trend. These processes smoothens the rough surface of the materials, and the performance of devices can improve dramatically. They are also used in novel machining approaches and diamond wheels to fabricate wafers, which are used in semiconductor and microelectronics industries. This is frequently carried out using environment friendly slurries making the process greener (Zhang et al. 2016a, b, 2019).

Owing to their large surface-to-volume ratio nanomaterials prove to be significantly attractive and highly efficient catalysts, especially transition metal nanomaterials (Patzke et al. 2011; Gawande et al. 2012). Lately, with so much advancement in nanotechnology, nanomaterials are looked upon as alternatives for almost all the traditional applications whether it is in research or industrial front. As a result they are being exploited in almost all possible branches of catalysis. It is worth mentioning that in recent literature, many nanomaterials are also explored for their enzyme-like activity as well (He et al. 2014; Golchin et al. 2017). To list down, some Au@Pt nanoparticles show oxidase-mimicking activity (Zhou et al. 2013), Fe_3O_4 magnetic nanoparticles and Fe–Co bimetallic alloy have peroxidase mimic activity (Wei and Wang 2008; Chen et al. 2013). CeO_2 has been reported to exhibit catalase and superoxide dismutase-like activity (Korsvik et al. 2007; Pirmohamed et al. 2010), Pt nanoparticles are reported as uricase mimic (Dong et al. 2011), and so on. Recently, Vernekar et al. have reported V_2O_5 nanowires as glutathione peroxidase mimic, $MnFe_2O_4$ as oxidase mimic and organo-telluride as mimic of glutathione peroxidase in catalytic reduction/decarboxylation of grapheme oxide as well (Vernekar and Mugesh 2013; Vernekar et al. 2014; 2016a, b). These are only a few of such artificial enzymes reports of late. The many advantages of these enzyme-like activity displaying nanoparticles or nanozymes, is the low production cost, controlled synthesis, tuneable catalytic activities and better stability to external conditions over their enzyme counterparts (Wei and Wang 2013). It would be no surprise if these nanozymes become rightful substituents in medical research for human welfare in the coming future.

Fascinated by this aspect of nano-catalysis, in our present study, we have investigated oxidase mimic activity of Co-doped MnO_2 nanozyme using 3,3′,5,5′-tetramethylbenzidine (TMB) as the model substrate and further applied it in oxidative degradation of uric acid as a solution for the condition of gout. The current investigation deals with degradation studies of uric acid over the synthesised 2% Co-doped MnO_2 by simple co-precipitation. The result clearly indicates better mimetic activity of these nanozyme over earlier reported uricase enzyme mimics as the activation energy of the reaction reduced from the reported value of 53 to 44 kJ mol^{-1}. In situ generation of singlet oxygen/superperoxide-type radical species is another striking feature of the used nanozyme. Analysis of the products revealed the pathway followed for the oxidative degradation over the synthesised nanozyme to be similar to uricase. We hence propose Co-doped MnO_2 as a cost effective and bio-relevant substituent for removal of excess uric acid from the body as well as an efficient nanozyme candidate for the treatment of gout.

Experimental

Materials and methods

For all experimental procedures, doubly distilled water was used. All chemicals used for catalyst synthesis and 1,3-diphenylisobenzofuran (DPBF) were obtained from Sigma Aldrich and used as it is. AR grade Uric acid was obtained from Kemphasol. TMB, NaCl, Na_2HPO_4, KCl, Phthalic acid and KH_2PO_4 used were commercially available reagent grade. The prepared catalyst sample was well characterised by IR spectroscopy recorded on Shimadzu IR prestige 21 spectrophotometer and XRD pattern recorded on a Rigaku diffractometer, using Cu Kα radiation ($\lambda = 1.5418$ Å, filtered through Ni filter) to obtain its structure and phase. The XPS analysis were carried out to determine surface composition with PHI5000 Versa Probe II model. The morphology of catalysts was determined using Zeiss Avo18 Scanning Electron Microscope (SEM). Particulate size confirmation and selected area electron diffraction (SAED) were carried out by Transmission

Electron Microscopy (TEM) using Philips CM 200 electron microscope (resolution = 2.4 Å). Energy-dispersive X-ray spectroscopy (EDS) were recorded on an Oxford instrument. All the kinetic reaction studies were monitored using Agilent tech UV–Vis Spectrophotometer. The mechanistic details were studied using Shimadzu RF-5301 PC Spectrophotofluorometer and Waters Acquity TQD LC–MS (liquid chromatography coupled with mass spectroscopy) featuring an ODS-2, 250 × 4.6, 5 µm column.

Preparation of Co-doped MnO_2 nanozyme

Co-doped MnO_2 was prepared via simple co-precipitation method. In brief, calculated amounts of Mn^{2+} and Co^{2+} salts were first dissolved in 100 mL of distilled water. This was co-precipitated using required amounts of hydroxide base added drop wise with constant stirring (pH 9). The obtained suspension was stirred vigorously for sometime before addition of 30% H_2O_2. Change in colour of the whole mixture to black was an indication of all Mn^{2+} being converted to Mn^{4+}. The mixture was allowed to stir for more than 3 h for homogeneity. The obtained solid was filtered off with copious amount of distilled water and dried overnight. On drying, the solid was ground well with a mortar and pestle and calcined at 400 °C for 10 h. The resulting solid was treated as Co-doped MnO_2.

Procedure for TMB oxidation by nanozyme

A 50 µM TMB solution was subjected to room temperature (RT) oxidation using 20 µg mL^{-1} of the catalyst sample. The reaction was carried out in citric acid buffer of pH ranging from 2.0 to 7.4. 10 mL of 50 µM TMB solution was taken in a modified cuvette with extended volume capacity and placed in the sample holder. The absorbance was recorded at 652 nm and 450 nm. To this was then added weighed amount of the nanozyme to make 20 µg mL^{-1} solution of it. Using the kinetic mode of the instrument, change in $A_{652\ nm}$ was measured for all the buffer samples for 10 min.

Procedure for uric acid degradation

A 50 µM solution of uric acid was prepared in phosphate buffer saline (PBS) of pH 7.4. Each test used 25 mL of this solution containing 50 µg mL^{-1} of the catalyst. The solution was stirred continuously at required temperature and aliquots were removed periodically to be analysed by UV spectrophotometer in the range 350–200 nm.

Procedure for hydroxy radical (·OH) and singlet oxygen ($^1O_2$) detection

Terephthalic acid (TA) and 1,3-diphenylisobenzofuran (DPBF) were used as probes for ·OH and $^1O_2$ detection, respectively. The catalyst 1 mg mL^{-1} was incubated for a minimum of 30 min before all the tests in PBS of pH 4, 7.4, 10 and distilled water at 37 °C separately. For ·OH detection, 2 mM TA solution was prepared in 5 mM NaOH. Typically, TA stock solution was taken in the cuvette to which 100 µL of catalyst-incubated buffer was added. This was then irradiated at 315 nm and its emission spectra were recorded simultaneously over spectrophotofluorometer. The catalyst-incubated buffers were centrifuged right before the tests (Liu et al. 2012; Bharathkumar et al. 2015).

For the detection of $^1O_2$, a fluorescent molecule, DPBF was used which is a specific $^1O_2$ quencher. As mentioned in the earlier case, here also DPBF exhibits fluorescence when irradiated at 410 nm (Carloni et al. 1993; Ohyashiki et al. 1999). Briefly, 3 µM solution of DPBF in EtOH was used for the experiment. The DPBF solution was introduced in the cuvette and added with 100 µL of catalyst-incubated buffer. The change in emission at 457 nm was noted.

Procedure for leaching and recyclability test

To check for metal leaching in the followed protocol for UA degradation, the formulated reaction was carried out at 37 °C for 2 h. The absorbance of the solution was measured before and after the said time. Half of it was filtered using Whatman paper 42 and both, the remaining half as well the filtrate (free of catalyst), continued to be stirred at 37 °C for another 2 h time before recording its absorbance. In addition, the ICP-AES data of the recovered sample was verified after four cycles. Additionally, the catalyst was successfully reused for four cycles without loss of its catalytic activity. For recyclability, the spent catalyst was simply filtered from the buffer solution using Whatman paper and washed with absolute ethanol followed by drying at 100 °C overnight before reuse.

Results and discussion

Catalyst characterisation

All the samples were prepared via simple co-precipitation of the metals followed by low-temperature calcination. This made sure that the resultant nanoparticles had smaller sizes and higher surface areas. An average crystallite size below 12 nm and surface area of 86.14 $m^2\ g^{-1}$ were obtained for the nanozyme $Mn_{0.98}Co_{0.02}O_2$. This was far better as compared to surface area of ~ 30 $m^2\ g^{-1}$ for the pristine. This increase in surface area was a consequence of cobalt doping in the MnO_2 lattice. Doping Co also resulted in facilitating more lattice oxygen as observed by the EDAX data (ESI) which proved beneficial for the oxidative conversion of UA. Beyond 2% Co doping, the surface area was found to

decrease. Figure 1c represents XRD pattern of the synthesised $Mn_{0.98}Co_{0.02}O_2$ catalyst. It very well matches α-MnO_2 (JCPDS card no. 44-0141) with $2\theta = 37.2°$ as the 100% intensity peak indicating it to be tetragonal in structure. The IR data as well indicate the absence of any organic moieties or hydroxyl linkages in the sample (Fig. S1).

The SEM and TEM images further confirm the morphology and size of the sample (Fig. 1a, b). TEM images clearly show rod-shaped particles of size below 10 nm in diameter. The SAED pattern (inset in Fig. 1b) accompanying the TEM data was used to calculate *d* values that very well could be indexed to the α-phase of MnO_2 obtained from the XRD (Fig. S2). The XRD pattern depicted in Fig. 1c matches very well with the SAED pattern. EDAX further confirmed the presence of intended metals in the system matching with the theoretical percentages and the elemental mapping showed uniform distribution of the same throughout the sample (ESI, Table S1). ICP-AES analysis revealed the total percentage of Co in the sample to be 1.9% which is a close match with the intended 2%. This confirmed the formation of the intended system $Mn_{0.98}Co_{0.02}O_2$.

XPS studies were carried out to know the exact oxidation states of the metals in the sample. Fig. S3 shows the survey scan indicative of all the metals present in the sample. The 2p region scan of Mn (Fig. 2a) shows distinctive $2p_{1/2}$ and $2p_{3/2}$ peaks at 653.6 eV and 643 eV, respectively. The peaks appearing on the higher side of the energy scale is an indication of Mn in +4 oxidation state. In addition, to confirm the same, we recorded Mn 3s multiplet splitting (Fig. 2b) value for the sample which mainly originates from the coupling effect of non-ionised 3s electrons with the 3d valence band electrons which amounted to 4.7 eV (Li et al. 2015).

The ΔE_{3s} values are inversely proportional to oxidation state of Mn atoms in Mn-containing oxides as established by Kim and co-authors, the average valence of the prepared sample is calculated to be +3.68 on the basis of $\Delta E_{3s} = 4.7$ eV which is close to +4 (Cerrato et al. 2010; Song et al. 2014). The Co 2p region scan (Fig. 2c) again

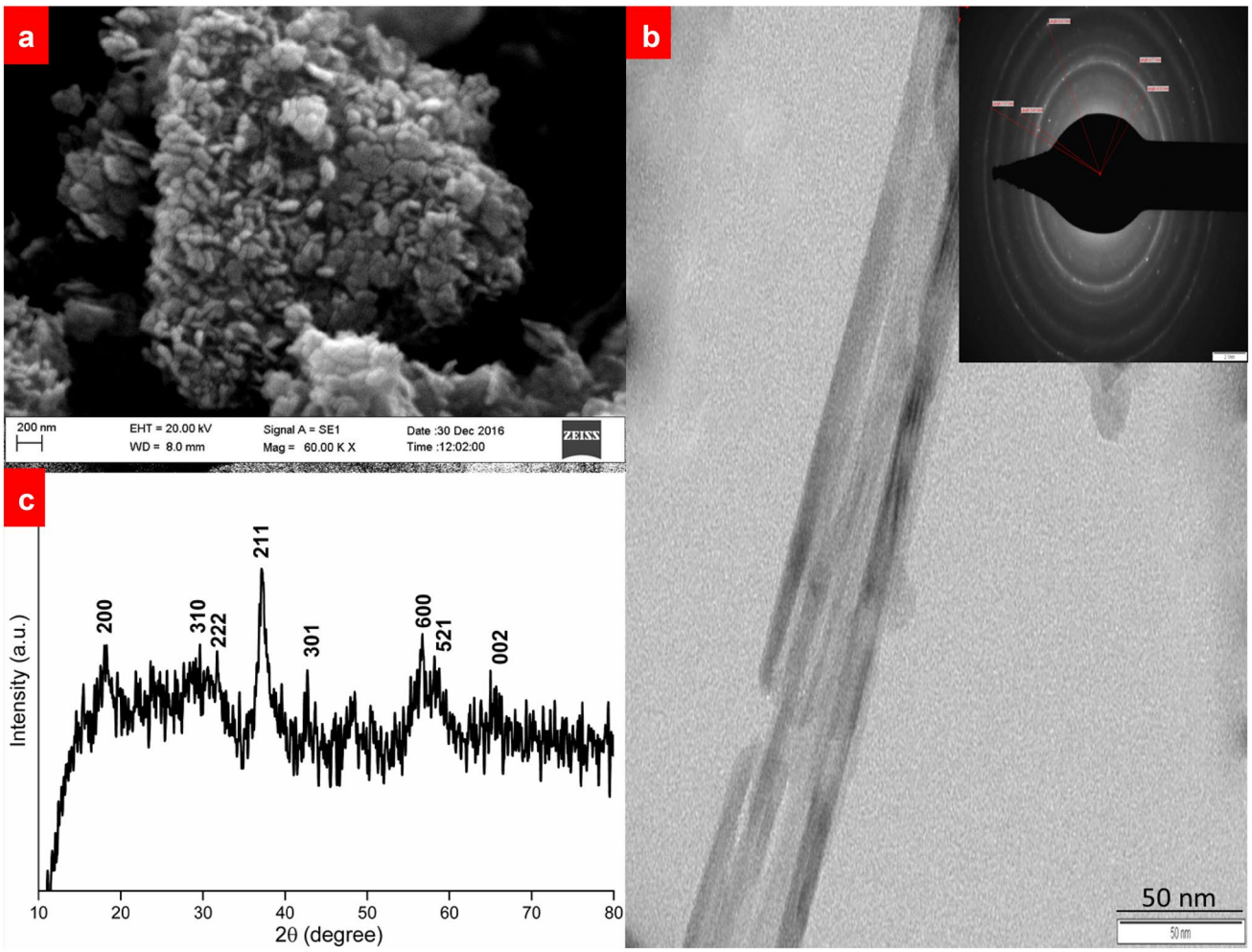

Fig. 1 SEM (**a**) and TEM (**b**) images of the synthesised sample $Mn_{0.98}Co_{0.02}O_2$, the rod-shaped morphology is clearly identifiable in it. The inset in **b** shows the SAED pattern of the sample. **c** is the obtained XRD powder pattern of the sample

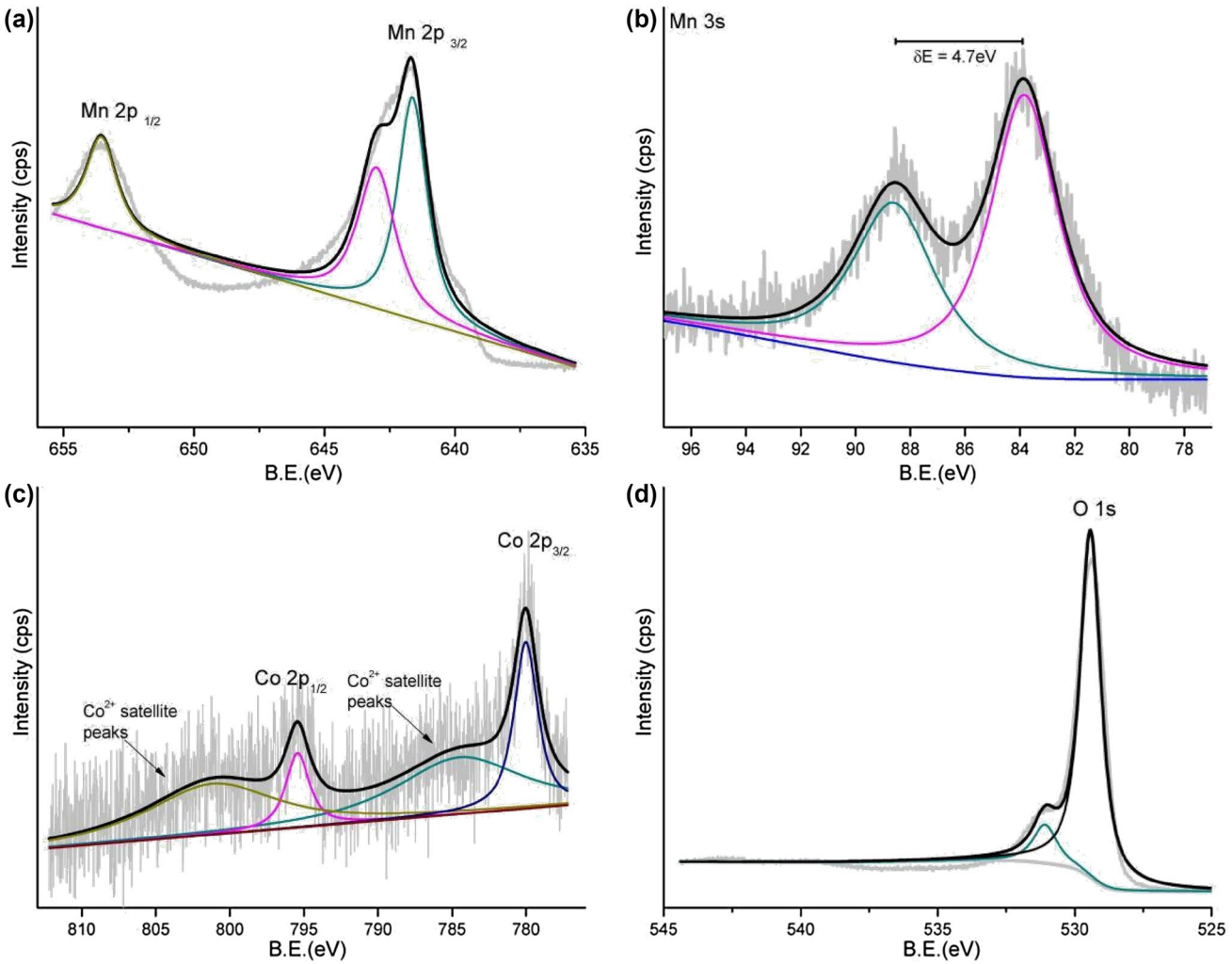

Fig. 2 XPS analysis of each individual element in the sample depicted in the figure. **a** and **b** are Mn 2p and 3s region scans indicating it to be present as Mn^{4+}, **c** is Co 2p region scan hinting it to be exclusively present as Co^{2+} and **d** is the O 1s scan for the sample

confirms the presence of Co in +2 oxidation state. This is clearly indicated by the two peaks at 780 eV and 795.5 eV, respectively, corresponding to $2p_{3/2}$ and $2p_{1/2}$ along with their satellites around 785 eV and 801 eV which are well matching to that in reports (Tan et al. 1991; Biesinger et al. 2011). The O 1s peak comes around 529.4 eV (Fig. 2d) which indicates the sample to be a metal oxide (Dupin et al. 2000). All the discussed data hence confirm the formation of the desired $Mn_{0.98}Co_{0.02}O_2$ nano-catalyst.

Catalytic activity

Uricase or urate oxidase is an oxidase enzyme responsible for the hydrolysis of uric acid to allantoin in the purine degradation pathway (Motojima et al. 1988). On establishing, the formation of the desired composition as described above, applicative studies carried out over the highly oxidative Co-doped MnO_2 sample. To exploit the oxidase-like property, TMB was used as the model substrate. The standard colour test was performed to determine the oxidative nature of the sample. A 50 µM TMB solution was subjected to RT oxidation using 20 µg mL^{-1} of the catalyst sample. The reaction was carried out in citric acid buffer of pH ranging from 2.0 to 7.4 (Fig. S4). Citrate buffer was preferred over phosphate buffer as the experiments run in an acidic pH range. The results depicted that the acidic pH of 4 showed the best activity as can be seen from Fig. S5a. It also resulted in formation of most intense blue colour (one electron oxidation of TMB) as compared to other buffers (Fig. S4). Once the oxidase-like property of the nanozyme was established by the above results, we used this nano-catalyst sample for mimicking uricase activity in oxidative degradation of UA.

The reaction was initially performed in phosphate buffer saline (PBS) of three different pH values of 4, 7.4 and 10 at 37 °C (ESI). Although the degradation was faster at pH 4, since our emphasis was more on to mimic the activity of

uricase enzyme, all the reactions were performed at physiological pH and temperature and therefore PBS of 7.4 was used. A 50 µM uric acid solution was used throughout the studies prepared in PBS of pH = 7.4 (physiological pH) and temperature conditions of 37 °C, unless mentioned otherwise. 25 mL of this solution was kept under vigorous stirring conditions for 24 h in a water bath, at 37 °C without any metal catalyst. The absorbance of the solution was measured at $\lambda = 291$ nm before and after indicated negligible change in the value, thus proving the UA solution to be stable in the employed conditions. Oxidative degradation was carried out in the exact same conditions in the presence of nanozyme.

Effect of nanozyme concentration

As the amount of catalyst was increased from 20 to 50 µg mL^{-1} of the solution, complete degradation of 50 µM uric acid at 37 °C was obtained within 4 h (Fig. 3). Further increase in catalyst concentration resulted in no more change in rate of the reaction (Fig. S5b). Thus, 50 µg mL^{-1} was found to be the optimum amount of catalyst for 50 µM uric acid solution at 37 °C. As the reaction followed first-order kinetics, plots of ln A_t/A_0 against time in minutes were plotted to calculate the rate constant (Parmekar and Salker 2016). The rate constant k for the reaction was found to be 1.208×10^{-4} s^{-1} at this temperature (Fig. 4a).

The reaction does not progress in the presence of H_2O_2 alone, without the catalyst. (Fig. 4c) In addition, individual metal ions Mn^{2+}, Mn^{3+}, Co^{2+}, $Mn^{2+} + Co^{2+}$ and Mn^{2+} with H_2O_2 were taken in 50 µM UA solution resulting in ~ 100 µg mL^{-1} of total metal in each case. It was treated to same standardised conditions of temperature and pH as followed for the oxidative degradation of UA with the nanozyme. Except for Mn^{2+} with H_2O_2, which showed marginal degradation, none other metal ion solution showed an appreciable decrease in the absorbance at λ_{max} of UA in 90-min time. This further proved that the reaction is heterogeneous in nature as well as indicated the necessity of maintaining a proper oxidation state of all the metals. The intended catalytic degradation requires the metals to be in specified oxidation state of + 4 and + 2 for Mn and Co, respectively. Even when compared with Mn–Co 1:1 composite, 10% Co supported MnO_2 and 10% Co-doped MnO_2, the doped sample showed the best outcome (plots not shown). As mentioned earlier, Co doping not only increased the surface area of the nanozyme but also increased the available oxygen. The role of it is however not well understood though, but we believe that it somehow aids in making more lattice oxygen available for catalyst surface thereby enhancing the oxidation property of the catalyst and aiding in uricase mimic activity of the nanozyme. When tested with same amounts but different concentration-doped Co, that is $Mn_{1-x}Co_xO_2$ ($x = 0.005$, 0.01, 0.02, 0.05 and 0.08), the rate was found not to increase further with more than 2% doping (Fig. 4d). The surface area also was somehow found to decrease with further increase in Co concentration. Thus, the sample $Mn_{0.98}Co_{0.02}O_2$ was chosen as the best composition to carry out detailed study.

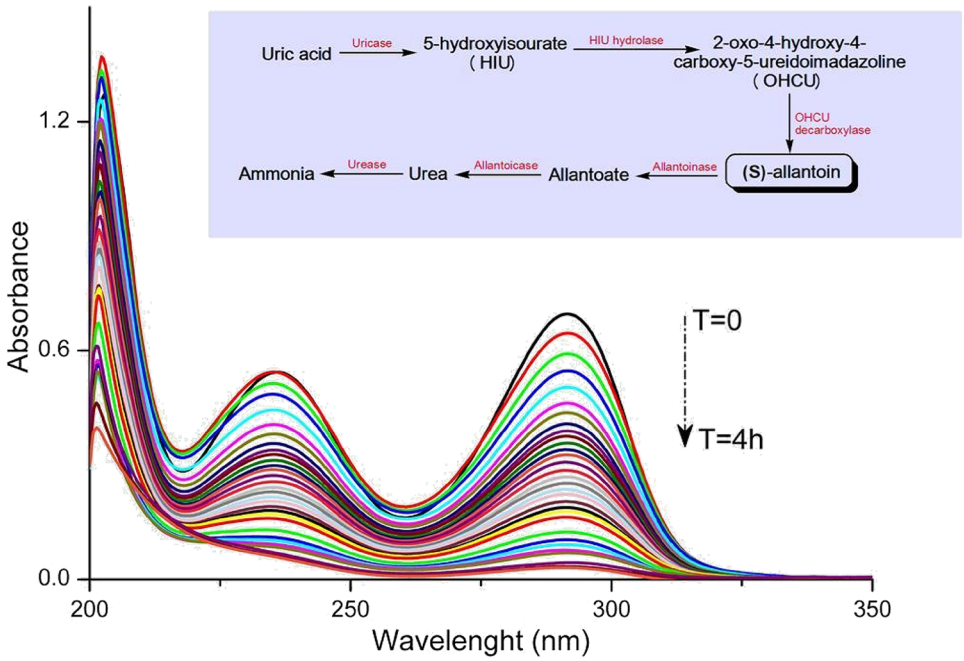

Fig. 3 The progressive degradation of uric acid can be seen in the figure with respect to time in minutes at $\lambda = 291$ nm. The initial decrease measured every 10 min for first 2 h and later every 15 min. The inset above shows the degradation scheme for UA in the presence of enzymes

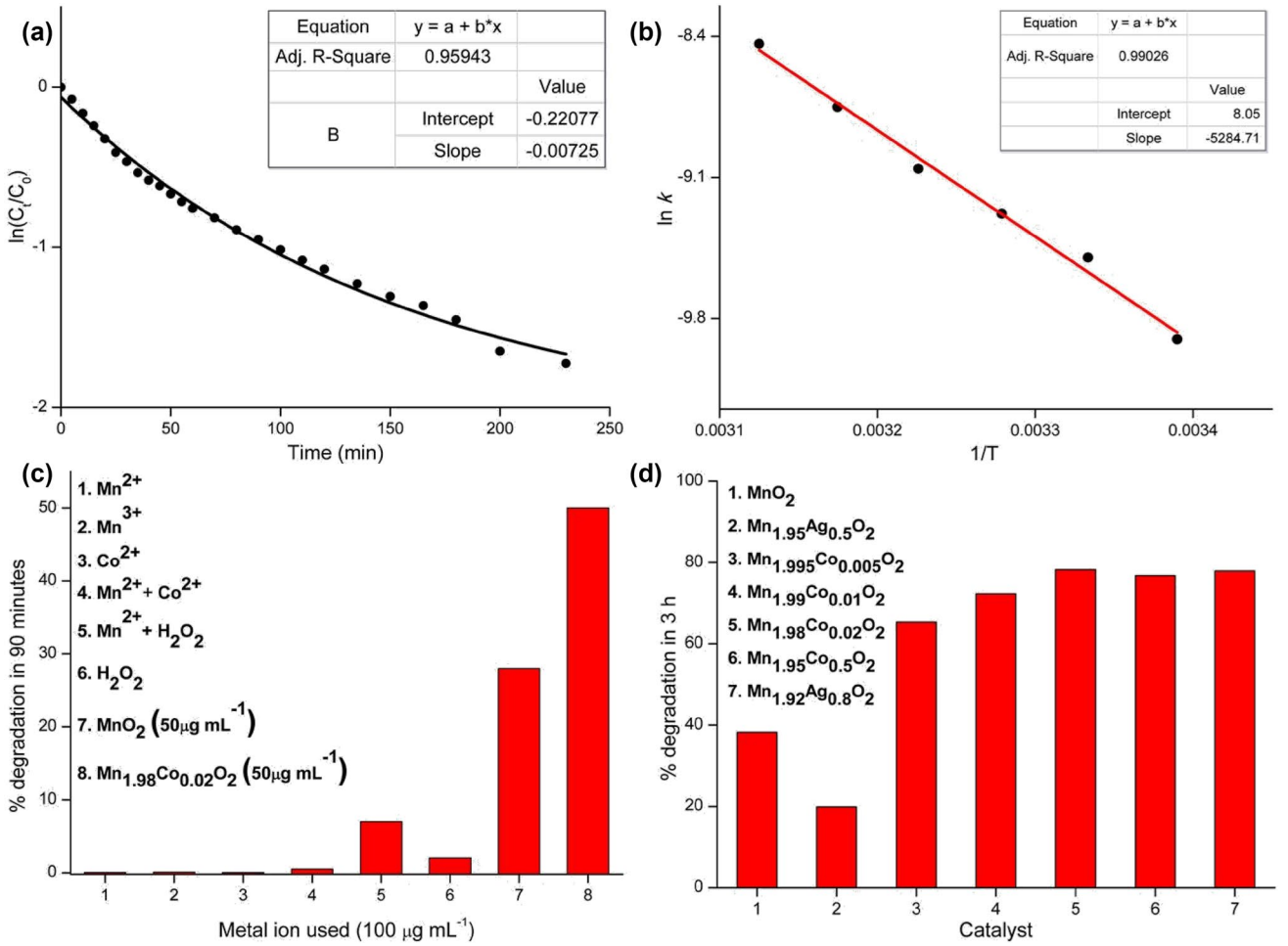

Fig. 4 **a** The first-order kinetic plot for calculating k for the degradation at 37 °C, **b** the Arrhenius plot of ln k vs. 1/T for calculating E_{act} of the reaction, **c** the obtained degradation of UA at 291 nm after 90-min time for different metal ions (100 µg mL^{-1}) and **d** the obtained degradation in 3 h over pristine and varied Co-doped MnO_2

Effect of temperature

Following Arrhenius concept, the rate of the reaction was found to increase with increase in temperature. The temperature gradient studies were carried out in the range 22–47 °C with 5 °C increase in temperature at each step, in the presence of the 50 µg mL^{-1} catalyst. The rate constant (k) reached as high as 2.167×10^{-4} s^{-1} at 47 °C. The average activation energy (E_{act}) reported for this reaction utilising bacterial uricase enzyme is 53 kJ mol^{-1} wherein the synthesised catalyst could lower it to 44 kJ mol^{-1} as calculated from plot of ln k vs 1/T (Fig. S5c) (Alamillo et al. 1991; Dong et al. 2011). This is much lower than what was found using Pt nanoparticles (PtNPs) as well (Dong et al. 2011). In addition, the E_{act} in the absence of the catalyst as reported in the same article is of the order 139 kJ mol^{-1} comparable to what was obtained for catalyst-free reactions in the temperature range of 30–50 °C (data not shown). Another advantage of the catalyst over PtNPs is that the major metal components of our proposed catalyst are manganese and cobalt, which are bio-relevant and organically present in our system. Mn is one of several first-row transition elements that have been employed by biological systems to assist in varied metabolic and structural roles (Law et al. 1998). It is essential for metabolization of cholesterol, carbohydrates and proteins along with being an integral part of the antioxidant enzyme superoxide dismutase (SOD) (Law et al. 1998). Co is essential element in humans as it exists at the core of cobalamine (vitamin B_{12}) (Yamada 2013). Thus, both the metals are bio-relevant and essential for normal functioning of the human body in contrast to PtNPs which is the only other nanozyme so far reported for similar uricase mimic activity. No other metal nano-catalyst or complex was reported to show such activity. PtNPs, however, are proven toxic as chronic exposure even at low concentration to it has been associated with asthma, dermatitis, and other serious

health problems in humans (Asharani et al. 2011; Konieczny et al. 2013; Sørensen et al. 2016).

Leaching and recyclability test

To find out if any metal leaching takes place in the followed protocol for UA degradation, the formulated reaction was carried out at 37 °C for 2 h. The absorbance of the solution was measured before and after and found to have degraded by almost 70% in the mentioned time. As mentioned in the experimental section, it was then separated into two halves. The half retained with the catalyst showed complete degradation of UA at the end of 4 h time in total whereas the filtrate reacted for an extended 2 h without catalyst showed no change in absorbance. This confirmed the fact that no leached metal from the catalyst was responsible for the oxidase property of the nanozyme, which was further proved by the ICP-AES data of the recovered sample showing negligible loss of metals after four cycles. Thus, in the employed reaction conditions, the reaction is exclusively heterogeneous in nature. Additionally, we could successfully reuse the catalyst for four cycles without loss of its catalytic activity. The TEM of the recovered sample was seen to sustain the morphology even after being reused (Fig. 5). Even EDAX showed negligible change in percent composition of the catalyst after reuse (ESI). Hence, we claim to have developed a recyclable system yielding the lowest E_{act} for oxidative degradation of UA as well as proposing it to be a promising contender as an enzyme mimic of uricase in the treatment of gout.

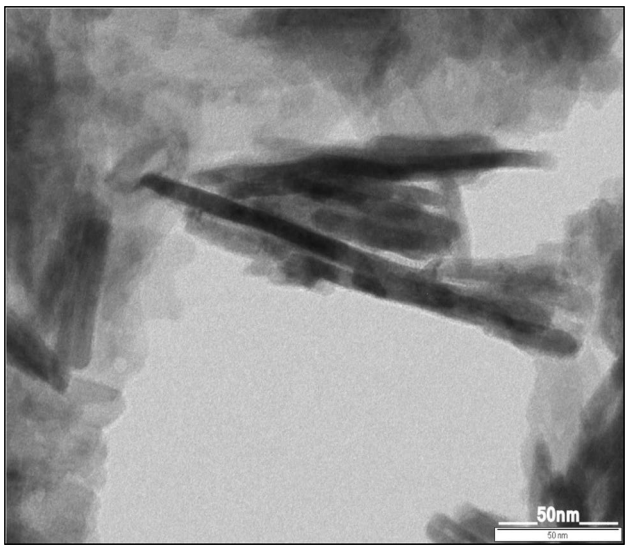

Fig. 5 TEM image of the recovered sample after four cycles

Mechanistic details of oxidative degradation of UA over Co-doped MnO_2

The nano-catalyst sample $Mn_{0.98}Co_{0.02}O_2$ with higher surface area as compared to all the other samples tested, proved most efficient as uricase mimic. Thus, it could be proposed that the sample exhibits surface catalysis. As discussed above, 50 µM UA solution when treated with 50 µg mL^{-1} concentration of the catalyst was found to degrade it to its molecular components within 4 h at 37 °C in PBS of pH 7.4. For the catalyst to be considered as a potential enzyme mimic for the treatment of gout, it is significant to know whether the pathway followed for degradation is the same as uricase enzyme or different. For this reason, it was indeed obligatory to study the course of UA degradation over the catalyst. Hence, factors, which might affect the activity like presence of oxygen, pH of the solution along with Michaelis–Menten constant (K_m) and maximum reaction rate (V_{max}) were determined. In addition, LC–MS data were recorded for the degraded sample to find out molecular composition of the degraded products.

Effect of dissolved oxygen and pH

Initially, the reaction was tested in PBS of 3 different pH values of 4, 7.4 and 10 at 37 °C. It was indeed interesting to note that the catalyst more facilitated in an acidic medium. As our aim was to mimic the uricase enzyme, physiological pH was used for the reaction studies. It is well known that most heterogeneous catalyst work by first adsorbing the reactant molecules over its surface. Once the reactants are in closer proximity, there is ease in reaction proceedings leading to product formation. As the reaction under consideration is oxidative in nature, it is but natural to assume that oxygen would play a vital role in its completion. To evident this hypothesis the reaction was carried out in a round-bottom flask, in total absence of molecular oxygen (O_2), by removing the atmosphere and dissolved gases from the flask using high vacuum and introducing argon (Ar) instead (ESI). Calculated amount of the catalyst was then added to the flask and placed in an ice jacket containing acetone to which liquid N_2 was slowly added resulting in freezing of the entire mixture (− 70 °C). The trapped gas molecules from this frozen mixture were then removed using very high vacuum. Still under Ar, the mixture was brought to room temperature and then placed in water bath at 37 °C. The mixture then subjected to vigorous stirring and its absorbance was recorded after 2 h of reaction time at this temperature, showing no change in absorbance at 291 nm (A_{291}) from the initial value. The reaction was carried out for 24 h, from the starting time at 37 °C under Ar and monitored using UV, only to confer that no change occurs in the A_{291} value in these conditions. After this time, the system was made

open to atmosphere and absorbance was measured after 2 h time. As expected, there was ~70% decrease in the A_{291} then what was obtained initially. This proves the importance of O_2 in exhibition of oxidase-like activity by the nanozyme. No activity was seen in the absence of catalyst or O_2, which proves that the oxidase activity is a synergistic action of both the nanozyme and O_2. Thus, it was confirmed that O_2 does take part in the reaction.

Confirmation of generated reactive oxygen species (ROS)

As reported in literature, metals such as Mn, Fe, and Co are known to convert O_2 to reactive oxygen species (ROS) which we assume happens in this case as well. Formation of ROS was confirmed by starch–iodide test yielding blue–violet coloration of the buffer only in the presence of the catalyst (ESI). As the starch–iodide test is blind to the actual reactive species which could be H_2O_2/·OH (hydroxide radical)/$\cdot O_2^-$ (superoxide radical) or $^1O_2$ (singlet oxygen), some simple tests were performed which could help us narrow down the choices. Specific tests for ·OH and $^1O_2/\cdot O_2^-$ were carried out using terephthalic acid (TA) and 1,3-diphenylisobenzofuran (DPBF), respectively (Wu et al. 2011; Bharathkumar et al. 2015).

Mechanistically, TA is non-fluorescent molecule which in the presence of ·OH forms 2-hydroxyterephthalic acid (HTA). This HTA when excited at 315 nm fluoresces at 425 nm (Bharathkumar et al. 2015). Using this principle, we performed the ·OH detection test. The catalyst-incubated buffers were centrifuged right before the tests. None of the tested samples showed fluorescence except for the reference one, which was incubated with Fe_3O_4 nanoparticles and externally added H_2O_2 (Fig. S6). This ascertained that no ·OH are formed in the reaction medium in the employed conditions. For the detection of $^1O_2/\cdot O_2^-$, a fluorescent molecule, DPBF was used which is a specific $^1O_2/\cdot O_2^-$ quencher.

As mentioned earlier, DPBF exhibits fluorescence when irradiated at 410 nm. In the presence of $^1O_2/\cdot O_2^-$, it forms endoperoxide by oxygen cycloaddition across the oxygen-sharing carbon atoms (C_2–C_5), resulting in non-fluorescent 1,2-dibenzoylbenzene (ODBB) (Inset in Fig. 6). When DPBF solution was introduced in the cuvette along with catalyst-incubated buffer, the decrease in emission at 457 nm was the indication of reaction of DPBF with $^1O_2/\cdot O_2^-$ resulting in ODBB (Fig. 6). A comparative time-based plot depicted in Fig. S8, showing change in emission intensity in the presence and absence of the nanozyme. This confirmed the formation of in situ singlet oxygen and/or superperoxide radical during the oxidation of UA in the presence of the nanozyme, which is basically responsible for its oxidase-like activity.

The reaction occurred within 10 min in all three buffer solutions of pH 4, 7.4 and 10. The reaction very much occurred in distilled deionised water as well which is suggestive of the fact that Cl^- plays no role in generation of the ROS and no halo-oxidase activity was exhibited by the catalyst. Thus, we conclude that the formation of $^1O_2/\cdot O_2^-$ is responsible for oxidase-like activity of Co-doped MnO_2 resulting in the oxidative conversion of UA to allantoin. In the process of oxidatively degrading UA, the nanozyme in

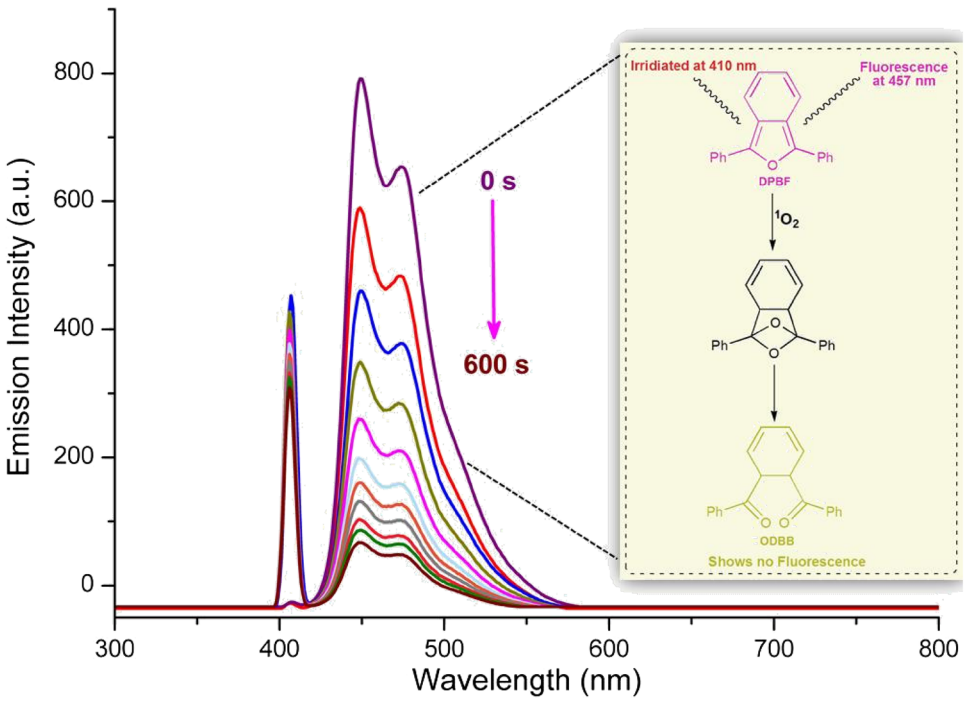

Fig. 6 Emission spectra obtained for with 3 µM DPBF due to formation of ODBB in the presence of catalyst-incubated buffer (pH 7.4) proving formation of $^1O_2/\cdot O_2^-$

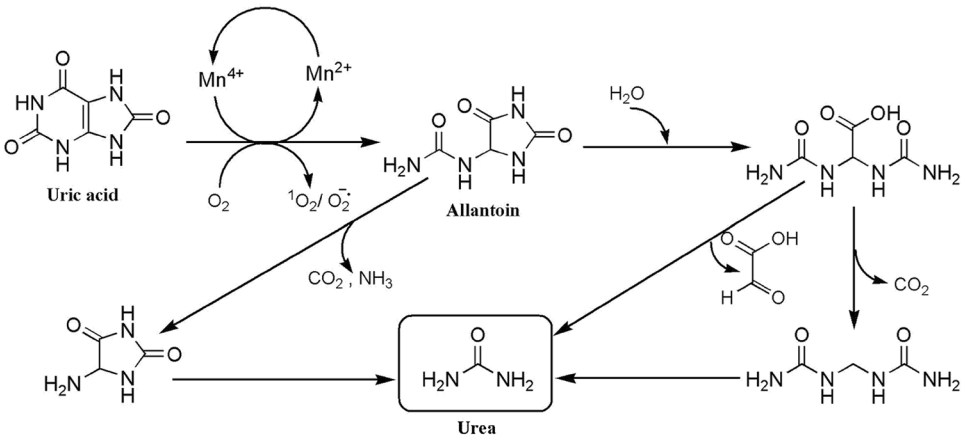

Scheme 1 Proposed pathway for degradation of uric acid over the catalyst based on the obtained LC–MS data

turn is reduced. This reduced catalyst is then regenerated utilising molecular O_2 from the air. Thus, molecular O_2 is utilised for generation of ROS as well as for oxidising the reduced catalyst in the last step and probably that is why the progress of reaction is dependent on it as previously established by under vacuum studies (Procedure is given in ESI, Fig. S5d).

Initial results showed TMB oxidation occurs with catalyst itself and no H_2O_2 is required to be added externally. In addition, a few drops of starch–iodide indicator with just the catalyst in acidified water gave intense violet coloration confirming formation of reactive oxygen species. Thereby, we can confidently say that the proposed nanozyme is an oxidase mimic and generates $^1O_2/\cdot O_2^-$ in situ in physiological medium (pH = 7.4) during the reaction.

K_m and V_{max} calculations for the UA degradation over the catalyst

Besides understanding the mechanism of surface electron transfer over the catalyst, the Michaelis–Menten behaviour of Co-doped MnO_2 nanozyme was also studied. Thus, kinetic parameters K_m and V_{max} were apparently acquired for UA degradation over the nanozyme using Lineweaver–Burk plot (Fig. S7). A low K_m represents high affinity between a substrate and the enzyme (Zhou et al. 2013). The obtained value of K_m of 22.34 µM is comparatively lower than what is previously reported for uricase enzyme (Cete et al. 2006). This demonstrates that Co-doped MnO_2 nanozyme is more reactive towards oxidative UA degradation and catalyses this enzymatic reaction faster than uricase. The obtained value of 0.00892 µM mL^{-1} for V_{max} also is lower than what was reported earlier for uricase.

Proposed pathway for oxidative decomposition of UA

The degraded solution of UA subjected to LC–MS analysis for understanding the pathway followed for oxidative degradation over the nanozyme. Three distinct peaks were observed in the HPLC chromatogram of the degraded sample, represented by the mass spectra corresponding to *m/z* values of 157, 114 and 61 (ESI). There was no trace of any peak at $m/z = 168$ signifying complete degradation of the parent substrate. Based on the obtained mass spectra of the products, we propose the following pathway for its degradation (Scheme 1). The peak at 157 and 61 are characteristic of allantoin and urea, respectively, both well-established water-soluble products of UA oxidation by uricase. Thus, we can very well say that degradation over our synthesised catalyst follows similar pathway as that of uricase enzyme in other mammals resulting in water-soluble products, hence verifying the fact that our proposed Co-doped MnO_2 nanozyme in reality acts like an enzyme mimic in the reaction.

Conclusion

In summary, a non-noble and cost-effective catalyst, 2% Co-doped MnO_2 was successfully synthesised using simple co-precipitation technique. The synthesised sample exhibited oxidase-like property when treated with TMB substrate to produce the colour test and hence was further studied for its oxidase-like property in degradation of UA. A 50 µM solution of UA could be completely degraded over 50 µg mL^{-1} of Co-doped MnO_2 nanozyme in PBS at physiological pH and temperature conditions. The kinetic studies further revealed a high rate constant *k* for the degradation reaction along with lowering the E_{act} by almost 9 kJ mol^{-1} in comparison with bacterial uricase. To the best of our knowledge 44 kJ mol^{-1} happens to be the lowest value of E_{act} reported for the degradation of UA by a mimic. By showing oxidase-like activity, the nanozyme $Mn_{0.98}Co_{0.02}O_2$ shows promising activity over wider pH range than a normal enzyme. In addition, the fact that it is able to generate in situ ROS-like $^1O_2/\cdot O_2^-$ can be put to use in cancer therapy as ROS-induced apoptosis is a known cancer treatment option. It can

also find use as antifouling agent without affecting marine biota as singlet oxygen is known to exhibit such antibacterial activity (Natalio et al. 2012; Zhou et al. 2017; Zhang et al. 2018). In this work, we could successfully propose a mechanistic pathway for the degradation over the nanozyme based on the obtained LC–MS data. Allantoin and urea were the predominant product of the degradation, both of which are water soluble. The major metal components of the proposed catalyst are manganese and cobalt, which biologically are present in humans making the whole study bio-relevant. Hence, we envision a bio-relevant, safe as well as inexpensive catalyst in the form of Co-doped MnO_2 nanozyme for efficient UA oxidative degradation and a potential treatment for the painful condition of gouty arthritis.

Acknowledgements We thank UGC, New Delhi for granting fellowship to MVP under BSR scheme. Thanks are due to Dr. Amit Vernekar, BITS, Hyderabad for the direction and valuable suggestions rendered during the entire study, Dr. S. N. Dhuri for extending the time-based UV–Vis facility sanctioned by DST, New Delhi (SR/FT/CS-006/2010) and Prof. P. Roy, Dept. of Zoology for making available the spectrophotofluorometry instrument. We gracefully thank SAIF IIT Bombay, IIT Kanpur, CDRI Lucknow, Birla Furukawa Verna and CSIR-NIO Donapaula for instrumental analysis.

Compliance with ethical standards

Conflict of interest On behalf of all the authors, the corresponding author states that there is no conflict of interest.

References

Abate N, Chandalia M, Cabo-Chan AV Jr et al (2004) The metabolic syndrome and uric acid nephrolithiasis: novel features of renal manifestation of insulin resistance. Kidney Int 65:386–392. https://doi.org/10.1111/j.1523-1755.2004.00386.x

Alamillo JM, Cfirdenas J, Pineda M (1991) Purification and molecular properties of urate oxidase from Chlamydomonas reinhardtii. Biochim Biophys Acta 1076:203–208

Asharani PV, Lianwu YI, Gong Z, Valiyaveettil S (2011) Comparison of the toxicity of silver, gold and platinum nanoparticles in developing zebrafish embryos. Nanotoxicology 5:43–54. https://doi.org/10.3109/17435390.2010.489207

Bharathkumar S, Sakar M, RV K, Balakumar S (2015) Versatility of electrospinning in the fabrication of fibrous mat and mesh nanostructures of bismuth ferrite (BiFeO3) and their magnetic and photocatalytic activities. Phys Chem Chem Phys 17:17745–17754. https://doi.org/10.1039/c5cp01640a

Biesinger MC, Payne BP, Grosvenor AP et al (2011) Resolving surface chemical states in XPS analysis of first row transition metals, oxides and hydroxides: Cr, Mn, Fe, Co and Ni. Appl Surf Sci 257:2717–2730. https://doi.org/10.1016/j.apsusc.2010.10.051

Carloni P, Damiani E, Greci L et al (1993) On the use of 1,3-diphenylisobenzofuran (DPBF). Reactions with carbon and oxygen centered radicals in model and natural systems. Res Chem Intermed 19:395–405. https://doi.org/10.1163/156856793x00181

Cerrato JM, Hochella MF, Knocke WR et al (2010) Use of XPS to identify the oxidation state of Mn in solid surfaces of filtration media oxide samples from drinking water treatment plants. Environ Sci Technol 44:5881–5886. https://doi.org/10.1021/es100547q

Cete S, Yasar A, Arslan F (2006) An amperometric biosensor for uric acid determination prepared from uricase immobilized in polypyrrole film. Artif Cells Nanomedicine Biotechnol 34:367–380. https://doi.org/10.1080/10731190600684116

Chen Y, Cao H, Shi W et al (2013) Fe–Co bimetallic alloy nanoparticles as a highly active peroxidase mimetic and its application in biosensing. Chem Commun 49:5013–5015. https://doi.org/10.1039/c3cc41569d

Dong Y, Chi Y, Lin X et al (2011) Nano-sized platinum as a mimic of uricase catalyzing the oxidative degradation of uric acid. Phys Chem Chem Phys 13:6319–6324. https://doi.org/10.1039/c0cp01759k

Dupin J, Gonbeau D, Vinatier P, Levasseur A (2000) Systematic XPS studies of metal oxides, hydroxides and peroxides. Phys Chem Chem Phys 2:1319–1324

Gawande MB, Pandey RK, Jayaram RV (2012) Role of mixed metal oxides in catalysis science—versatile applications in organic synthesis. Catal Sci Technol 2:1113–1125. https://doi.org/10.1039/c2cy00490a

Gersch C, Palii SP, Kim KM et al (2008) Inactivation of nitric oxide by uric. acid Nucleosides Nucleotides Nucleic Acids 27:967–978. https://doi.org/10.1080/15257770802257952

Golchin J, Golchin K, Alidadian N et al (2017) Nanozyme applications in biology and medicine: an overview. Artif Cells Nanomedicine Biotechnol 45:1069–1076. https://doi.org/10.1080/21691401.2017.1313268

He W, Wamer W, Xia Q et al (2014) Enzyme-like activity of nanomaterials. J Environ Sci Heal Part C 32:186–211. https://doi.org/10.1080/10590501.2014.907462

Konieczny P, Goralczyk AG, Szmyd R et al (2013) Effects triggered by platinum nanoparticles on primary keratinocytes. Int J Nanomedicine 8:3963–3975

Korsvik C, Patil S, Seal S, Self WT (2007) Superoxide dismutase mimetic properties exhibited by vacancy engineered ceria nanoparticles. Chem Commun. https://doi.org/10.1039/b615134e

Law NA, Caudle MT, Pecoraro VL (1998) Manganese redox enzymes and model systems: properties, structures, and reactivity. In: Advances in inorganic chemistry. pp 305–440

Li J-Y, Wu X-L, Zhang X-H et al (2015) Romanechite-structured Na0.31MnO1.9 nanofibers as high-performance cathode material for a sodium-ion battery. Chem Commun 51:14848–14851. https://doi.org/10.1039/C5CC05739F

Lippi G, Montagnana M, Franchini M et al (2008) The paradoxical relationship between serum uric acid and cardiovascular disease. Clin Chim Acta 392:1–7. https://doi.org/10.1016/j.cca.2008.02.024

Liu X, Wang Q, Zhao H et al (2012) BSA-templated MnO2 nanoparticles as both peroxidase and oxidase mimics. Analyst 137:4552. https://doi.org/10.1039/c2an35700c

Motojima K, Kanaya S, Goto S (1988) Cloning and sequence analysis of cDNA for rat liver uricase. J Biol Chem 263:16677–16681

Natalio F, André R, Hartog AF et al (2012) Vanadium pentoxide nanoparticles mimic vanadium haloperoxidases and thwart biofilm formation. Nat Nanotechnol 7:530–535. https://doi.org/10.1038/nnano.2012.91

Ohyashiki T, Nunomura M, Katoh T (1999) Detection of superoxide anion radical in phospholipid liposomal membrane by fluorescence quenching method using 1,3-diphenylisobenzofuran. Biochim Biophys Acta—Biomembr 1421:131–139. https://doi.org/10.1016/S0005-2736(99)00119-4

Parmekar MV, Salker AV (2016) Room temperature complete reduction of nitroarenes over a novel Cu/SiO2@NiFe2O4 nano-catalyst

in an aqueous medium—a kinetic and mechanistic study. RSC Adv 6:108458–108467. https://doi.org/10.1039/C6RA21942J

Patzke GR, Zhou Y, Kontic R, Conrad F (2011) Oxide nanomaterials: synthetic developments, mechanistic studies, and technological innovations. Angew Chemie—Int Ed 50:826–859. https://doi.org/10.1002/anie.201000235

Perez-ruiz F, Calabozo M, Pijoan JI et al (2002) Effect of urate-lowering therapy on the velocity of size reduction of tophi in chronic gout. Arthritis Care Res 47:356–360. https://doi.org/10.1002/art.10511

Pirmohamed T, Dowding JM, Singh S et al (2010) Nanoceria exhibit redox state-dependent catalase mimetic activity. Chem Commun 46:2736–2738. https://doi.org/10.1039/b922024k

Polshettiwar V, Varma RS (2010) Green chemistry by nano-catalysis. Green Chem 12:743–754. https://doi.org/10.1039/b921171c

Ramazzina I, Folli C, Secchi A et al (2006) Completing the uric acid degradation pathway through phylogenetic comparison of whole genomes. Nat Chem Biol 2:144–148. https://doi.org/10.1038/nchembio768

Shi Y, Evans JE, Rock KL (2003) Molecular identification of a danger signal that alerts the immune system to dying cells. Nature 425:516–521. https://doi.org/10.1038/nature01991

Song J, Gim J, Kim S et al (2014) A sodium manganese oxide cathode by facile reduction for sodium batteries. Chem—An Asian J 9:1550–1556. https://doi.org/10.1002/asia.201301510

Sørensen SN, Engelbrekt C, Lu HH et al (2016) A multimethod approach for investigating algal toxicity of platinum nanoparticles. Environ Sci Technol 50:10635–10643. https://doi.org/10.1021/acs.est.6b01072

Tan J, Klabunde KJ, Sherwood PMA (1991) XPS studies of solvated metal atom dispersed catalysts. evidence for layered cobalt-manganese particles on alumina and silica. J Am Chem Soc 113:855–861

Usuda N, Hayashi S, Fujiwara S et al (1994) Uric acid degrading enzymes, urate oxidase and allantoinase, are associated with different subcellular organelles in frog liver and kidney. J Cell Sci 107:1073–1081

Vernekar AA, Mugesh G (2013) Catalytic reduction of graphene oxide nanosheets by glutathione peroxidase mimetics reveals a new structural motif in graphene oxide. Chem—A Eur J 19:16699–16706. https://doi.org/10.1002/chem.201303339

Vernekar AA, Sinha D, Srivastava S et al (2014) An antioxidant nanozyme that uncovers the cytoprotective potential of vanadia nanowires. Nat Commun 5:1–13. https://doi.org/10.1038/ncomms6301

Vernekar AA, Das T, Ghosh S, Mugesh G (2016a) A remarkably efficient $MnFe_2O_4$ -based oxidase nanozyme. Chem−An Asian J 11:72–76. https://doi.org/10.1002/asia.201500942

Vernekar AA, Das T, Mugesh G (2016b) Vacancy-engineered nanoceria: enzyme mimetic hotspots for the degradation of nerve agents. Angew Chemie Int Ed 55:1412–1416. https://doi.org/10.1002/anie.201510355

Wang B, Zhang Z, Chang K et al (2018) New deformation-induced nanostructure in silicon. Nano Lett 18:4611–4617. https://doi.org/10.1021/acs.nanolett.8b01910

Wei H, Wang E (2008) Fe_3O_4 magnetic nanoparticles as peroxidase mimetics and their applications in H_2O_2 and glucose detection. Anal Chem 80:2250–2254. https://doi.org/10.1021/ac702203f

Wei H, Wang E (2013) Nanomaterials with enzyme-like characteristics (nanozymes): next-generation artificial enzymes. Chem Soc Rev 42:5981–6202. https://doi.org/10.1039/c3cs35486e

Wu H, Song Q, Ran G et al (2011) Recent developments in the detection of singlet oxygen with molecular spectroscopic methods. Trends Anal Chem 30:133–141. https://doi.org/10.1016/j.trac.2010.08.009

Yamada K (2013) Cobalt: its role in health and disease. In: Sigel A, Sigel H, Sigel RKO (eds) Springer, Dordrecht, pp 295–320

Zhang Z, Wang B, Zhou P et al (2016a) A novel approach of chemical mechanical polishing for cadmium zinc telluride wafers. Sci Rep 6:1–7. https://doi.org/10.1038/srep26891

Zhang Z, Wang B, Zhou P et al (2016b) A novel approach of chemical mechanical polishing using environment-friendly slurry for mercury cadmium telluride semiconductors. Sci Rep 6:1–9. https://doi.org/10.1038/srep22466

Zhang Z, Cui J, Wang B et al (2017) A novel approach of mechanical chemical grinding. J Alloys Compd 726:514–524. https://doi.org/10.1016/j.jallcom.2017.08.024

Zhang Y, Wang F, Liu C et al (2018) Nanozyme decorated metal-organic frameworks for enhanced photodynamic therapy. ACS Nano 12:651–661. https://doi.org/10.1021/acsnano.7b07746

Zhang Z, Cui J, Zhang J et al (2019) Environment friendly chemical mechanical polishing of copper. Appl Surf Sci 467–468:5–11. https://doi.org/10.1016/j.apsusc.2018.10.133

Zhou Y, He W, Wamer WG et al (2013) Enzyme-mimetic effects of gold@platinum nanorods on the antioxidant activity of ascorbic acid. Nanoscale 5:1583–1591. https://doi.org/10.1039/c2nr33072e

Zhou Z, Song J, Tian R et al (2017) Activatable singlet oxygen generation from lipid hydroperoxide nanoparticles for cancer therapy. Angew Chemie Int Ed 56:6492–6496. https://doi.org/10.1002/anie.201701181